ELSEVIER

Thermochimica Acta 390 (2002) 93–102

thermochimica acta

www.elsevier.com/locate/tca

Effects of inorganic components on the structure and thermo-oxidative degradation of PMMA modified metal alkoxide–EAA complex

T.C. Chang[a,*], Y.T. Wang[a], Y.S. Hong[a], Y.S. Chiu[b]

[a]*Department of Applied Chemistry, Chung Cheng Institute of Technology, NDU Tahsi, Taoyuan 335, Taiwan, ROC*
[b]*Chemical Systems Research Division, Chung Shan Institute of Science and Technology, Taoyuan 325, Taiwan, ROC*

Received 5 February 2002; accepted 11 February 2002

Abstract

Poly(methyl methacrylate) (PMMA) modified titanium and zirconium *n*-butoxide–ethyl acetoacetate (EAA) complex [M5-Ti$(OBu^n)_2(EAA)_2$ and M5-Zr$(OBu^n)_2(EAA)_2$] were obtained from trialkoxysilane-functional PMMA and EAA modified titanium and zirconium alkoxide via the sol–gel method. Infrared (IR), ^{13}C nuclear magnetic resonance (NMR) spectroscopy, and thermogravimetric analysis (TGA) were used to analyze the structures and properties of the hybrids with various proportions of metal oxide species. The effect of the complex of metal oxides and EAA ligands on structure and thermo-oxidative degradation of the M5-Ti$(OBu^n)_2(EAA)_2$ and M5-Zr$(OBu^n)_2(EAA)_2$ hybrids were investigated in this study. The ^1H spin–diffusion path length of the hybrids was in a nanometer scale as estimated from the spin–lattice relaxation time in a rotating frame ($T^H_{1\rho}$). The apparent activation energies (E_a), evaluated by van Krevelen's method, for random scission of PMMA segments in hybrids decreased with increasing metal oxide content.

Keywords: Poly(methyl methacrylate); Metal alkoxide; Hybrids; Relaxation; Degradation

1. Introduction

Purely inorganic sol–gel derived materials have been synthesized and investigated extensively for optical applications [1,2]. However, the solely inorganic materials can be very porous unless accompanied by high temperature densification. Thus, the materials prepared possibly have low optical and mechanical properties, since a large shrinkage during the thermal densification process can easily cause cracking.

An attractive method to overcome these problems is the use of organically modified silane (ORMOSIL) precursors via sol–gel process that involves hydrolysis and condensation reaction to form inorganic metal oxides network. The typical examples can produce TiO_2/ORMOSIL composite film [3,4] and SiO_2/TiO_2/ORMOSIL film [5]. The final materials have improved optical and mechanical properties. Zhang et al. used allyl acetylacetone as chelating agent to prepare the transparent poly(methyl methacrylate)–titania hybrids (PMMA–TiO_2) by sol–gel process [6]. Although allyl acetylacetone prevents the aggregation of particle, it still retains in the hybrid and would affect the optical properties. Chen et al. then used 3-(methacryloxy)-propyl trimethoxysilane (MSMA) as coupling agent to

* Corresponding author. Tel.: +886-3-389-1716; fax: +886-3-389-2711.
E-mail address: techuan@ccit.edu.tw (T.C. Chang).

0040-6031/02/$ – see front matter
PII: S0040-6031(02)00078-3

prepare the transparent poly(methyl methacrylate)–titania hybrids, P(MMA-MSMA)–TiO_2. They demonstrated the hybrid materials had a strong chemical bonding between the PMMA segment and the TiO_2 network, and there was no phase separation in the hybrid [7].

In our previous work, we prepared the poly(methyl methacrylate)–aluminum–ethyl acetoacetate [M5-Al(OBu^s)$(EAA)_2$] hybrids. We found that the first thermo-oxidative degradation stage in the hybrid was resulted from the EAA segments, and the apparent activation energy E_a for random scission of EAA decreased roughly with increasing the PMMA content [8]. In order to realize the influence of the complex of metal oxides and EAA ligand on structure and thermo-oxidative degradation of the hybrids, poly(methyl methacrylate) containing titanium or zirconium–ethyl acetoacetate hybrid materials, M5-Ti(OBu^n)$_2(EAA)_2$ and M5-Zr(OBu^n)$_2(EAA)_2$, were further prepared by the sol–gel technique in this work. To understand the interaction between metal oxide networks and PMMA or EAA segment in the hybrids, the proton spin–lattice relaxation times in the rotating frame ($T_{1\rho}^{H}$) of the hybrids were measured. On the other hand, the thermo-oxidative stability of the PMMA in the hybrids containing various proportions of metal oxides was measured by thermogravimetric analysis (TGA). The values of apparent activation energy (E_a) for random scission of PMMA segments in hybrids were evaluated by van Krevelen's method [9].

2. Experimental

2.1. Materials

The monomer methyl methacrylate (MMA, Janssen) was purified by distillation before use and [3-(methacryloxy)propyl] trimethoxysilane (MSMA, TCI) was used without purification. Titanium and zirconium *n*-butoxide [Ti(OBu^n)$_4$ and Zr(OBu^n)$_4$, Strem] was used as the inorganic source and it is commercially available. Ethyl acetoacetate (EAA, Janssen) was used as a chemical modifier of metal alkoxide in order to prevent the precipitation on the hydrolysis of metal alkoxide. Azobisisobutyronitrile (AIBN, BDH) was recrystallized from ethanol prior to use. Tetrahydrofuran (THF, Aldrich) was fractionally distilled in the presence of metallic sodium and benzophenone under nitrogen atmosphere. Deionized water (18 MΩ) was used for the hydrolysis.

2.2. Preparation of hybrids

PMMA containing titanium– and zirconium–EAA [M5-Ti(OBu^n)$_2(EAA)_2$ and M5-Zr(OBu^n)$_2(EAA)_2$], were prepared in situ by sequential synthesis, as shown in Scheme 1. In a typical example, a mixture of MMA (4.00 g) and MSMA (0.524 g), AIBN (6.89×10^{-3} g), and THF (28 ml) was poured into a 250 ml round bottom flask under nitrogen, and the solution stirred 24 h at 60 °C to initiate the copolymerization of the methacrylic monomers. A homogeneous solution of Ti(OBu^n)$_4$ (6.786 g) and EAA (5.19 g) was added, followed by addition of water (0.718 g) and ethanol (3.669 g). After stirring for 30 min at room temperature, the mixture was allowed to gel at room temperature for a week. The hybrid was further heated for 24 h at 70 °C, 3 h at 100 °C, and finally 24 h at 150 °C under vacuum. Hybrid M5-Ti(OBu^n)$_2(EAA)_2$-60 was obtained, where 60 donates that 60 wt.% of Ti(OBu^n)$_4$ based on weight of monomer (MMA and MSMA) and Ti(OBu^n)$_4$ condenses with 40 wt.% of PMMA with 5 mol% trialkoxysilyl-functional group. The formulations of the other hybrids are listed in Table 1.

2.3. Characterization of hybrids

The IR spectrum of the samples dispersed in dry KBr pellets were recorded between 4000 and 500 cm^{-1}. The ^{13}C nuclear magnetic resonance (NMR) spectra of the solid state M5-Ti(OBu^n)$_2(EAA)_2$ and M5-Zr(OBu^n)$_2(EAA)_2$ hybrids were measured using a Bruker MSL-400 with the cross-polarization combined with magic angle spinning (CP/MAS). The proton spin–lattice relaxation times in the rotating frame ($T_{1\rho}^{H}$) were measured by using a ^1H spin–lock τ-pulse sequence followed by cross-polarization. The ^1H 90° pulse width was 4.5 μs, and the CP contact time was 2 ms. The length of delay time, τ ranged from 0.1 to 25 ms for $T_{1\rho}^{H}$. The thermal stability of hybrid was measured using a Perkin-Elmer TGA-2 at heating rate of 10 °C/min in air and nitrogen. The sample weight was about 10 mg, and the gas flow rate was kept at 100 cm^3/min.

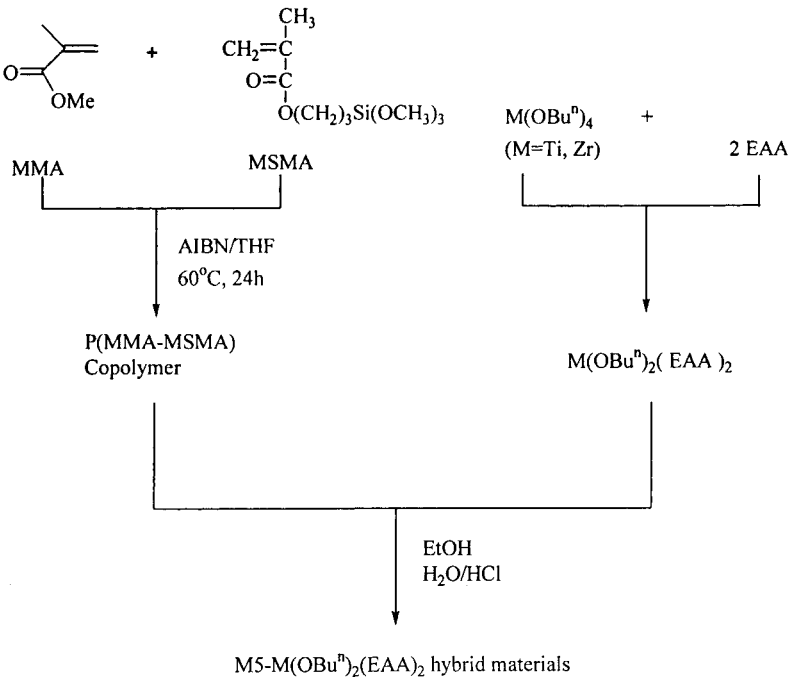

Scheme 1.

Table 1
Experimental conditions for hybrids

Hybrids	P(MMA-MSMA) (wt.%)	$M(OBu^n)_2(EAA)_2$ (wt.%)
(A) M5-$Ti(OBu^n)_2(EAA)_2$-30	70	30
(B) M5-$Ti(OBu^n)_2(EAA)_2$-60	40	60
(C) M5-$Ti(OBu^n)_2(EAA)_2$-85	15	85
(D) M5-$Zr(OBu^n)_2(EAA)_2$-30	70	30
(E) M5-$Zr(OBu^n)_2(EAA)_2$-60	40	60
(F) M5-$Zr(OBu^n)_2(EAA)_2$-85	15	85

[MSMA]/[MSMA] + [MMA] = 0.05; MMA: methyl methacrylate; MSMA: [3-(methacryloxy)propyl]trimethoxysilane; $Ti(OBu^n)_4$: titanium *n*-butoxide; $Zr(OBu^n)_4$: zirconium *n*-butoxide; EAA: ethyl acetoacetate; $M(OBu^n)_4$/EAA molar ratio = 1:2.

3. Results and discussion

3.1. Hybrids characterization

Fig. 1 shows the IR spectra of the M5-$Ti(OBu^n)_2(EAA)_2$ and M5-$Zr(OBu^n)_2(EAA)_2$ hybrids containing various proportions of PMMA. The broad band at 3100–3600 cm^{-1} is assigned to stretching vibrations of M–OH bonds (M = Ti or Zr), and the intensity of the peak increases with increasing TiO_2 or ZrO_2 content. The M–OH bonds observed here may be exhibit hydrogen bonding with the carbonyl group of the MMA moiety [7]. Stretching vibrations bands of the C–H, C=O and C–O–C or Si–O–Si bonds are observed at 2950, 1722 and 1144 cm^{-1}. Absorption peak at 1607 and 1531 cm^{-1}, respectively corresponds to C–O and C=C stretching vibration in the enol form of EAA bonded to $Ti(OBu^n)_4$ and $Zr(OBu^n)_4$ [10]. The results indicate that the EAA is complexed to metal alkoxides in the enol form. Moreover, the intensities of those peaks increase with increasing metal oxide content, suggesting that there is a greater chelating

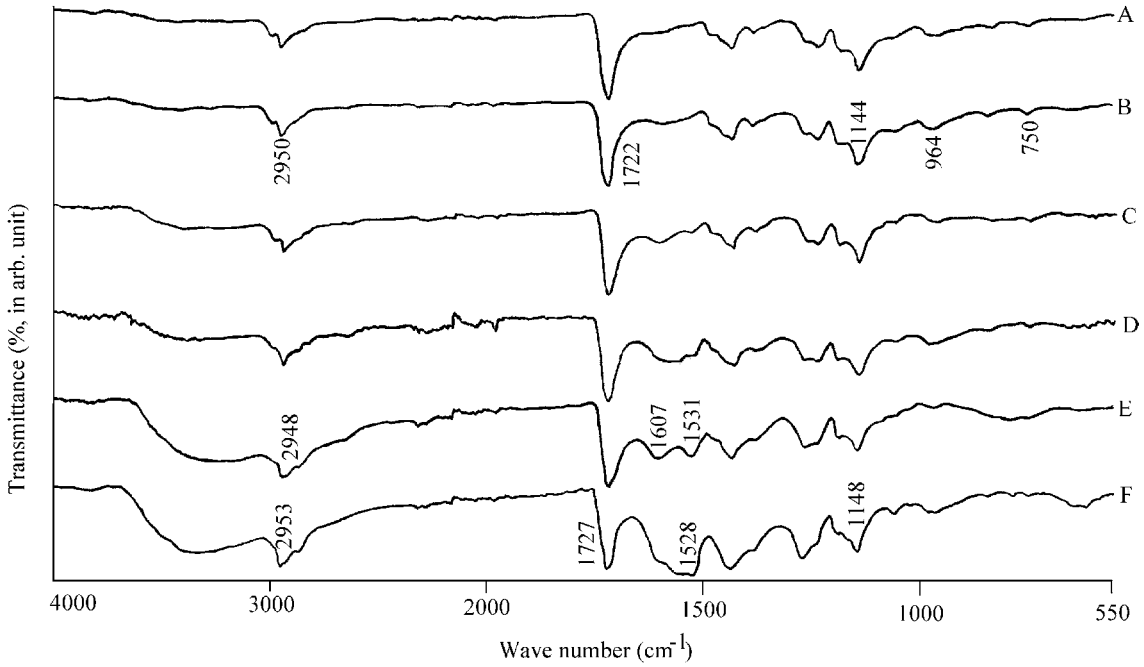

Fig. 1. Infrared spectra of the hybrids: (A) M5-Ti(OBu^n)$_2$(EAA)$_2$-30; (B) M5-Zr(OBu^n)$_2$(EAA)$_2$-30; (C) M5-Ti(OBu^n)$_2$(EAA)$_2$-60; (D) M5-Zr(OBu^n)$_2$(EAA)$_2$-60; (E) M5-Ti(OBu^n)$_2$(EAA)$_2$-85; (F) M5-Zr(OBu^n)$_2$(EAA)$_2$-85.

of EAA to the metal oxide network. On the other hand, those peak's intensities are in the order M5-Ti(OBu^n)$_2$(EAA)$_2$ < M5-Zr(OBu^n)$_2$(EAA)$_2$ hybrids. The results may be due to the more positive charge and the higher coordination number of the latter metal atom [11].

Fig. 2 shows the ^{13}C CP/MAS NMR spectrum of M5-Ti(OBu^n)$_2$(EAA)$_2$-85 and M5-Zr(OBu^n)$_2$(EAA)$_2$-85 hybrid. The chemical shifts for the PMMA segments observed at 178, 56, 52, 45 and 18 ppm correspond with the carboxyl, methylene, methoxy, quaternary and methyl carbons, respectively [12,13]. Therefore, the chemical shifts at 174, 85, 62, 24 and 15 ppm are due to the EAA ligand carbons. The resonance at 174 ppm is attributed to carbonyl carbons in enol form of EAA chelating to titanium or zirconium, while those at 85, 62, 24 and 15 ppm correspond to =C<u>H</u>–, –O<u>C</u>H$_2$CH$_3$, –C<u>C</u>H$_3$, and OCH$_2$<u>C</u>H$_3$, respectively [12,13]. Moreover, the ratio of intensity of the carbonyl carbon peak (I_{174}/I_{178}) in Fig. 2B is greater than that in Fig. 2A. It indicates that the latter has a more residual EAA segment, corresponding with the data of IR spectra.

3.2. Hybrids relaxation time

Based on the spin-locking mode employed in $T_{1\rho}^{H}$ measurement, the magnetization of resonance is expected to decay according to the following exponential function [14]:

$$M_\tau = M_0 \exp\left[-\tau/T_{1\rho}^{H}\right] \quad (1)$$

Here τ is the delay time used in the experiment and M_τ corresponds to resonance intensity. Fig. 3 shows the effect of delay time, τ on the ^{13}C resonance of the M5-Ti(OBu^n)$_2$(EAA)$_2$-85 hybrid. All the peaks present the same relaxation behavior, indicating no bias due to local environment. The $T_{1\rho}^{H}$ values of the respective carbon in the M5-Ti(OBu^n)$_2$(EAA)$_2$-60 and M5-Zr(OBu^n)$_2$(EAA)$_2$-60 hybrid can be measured by using the standard pulse sequence, as shown in Figs. 4 and 5, respectively. Moreover, the linear curves suggest that large-scale phase separation does not occur in hybrids. The $T_{1\rho}^{H}$ values of the M5-Ti(OBu^n)$_2$(EAA)$_2$ hybrid are around the same, are not affected by metal oxide content, while that of the M5-Zr(OBu^n)$_2$(EAA)$_2$

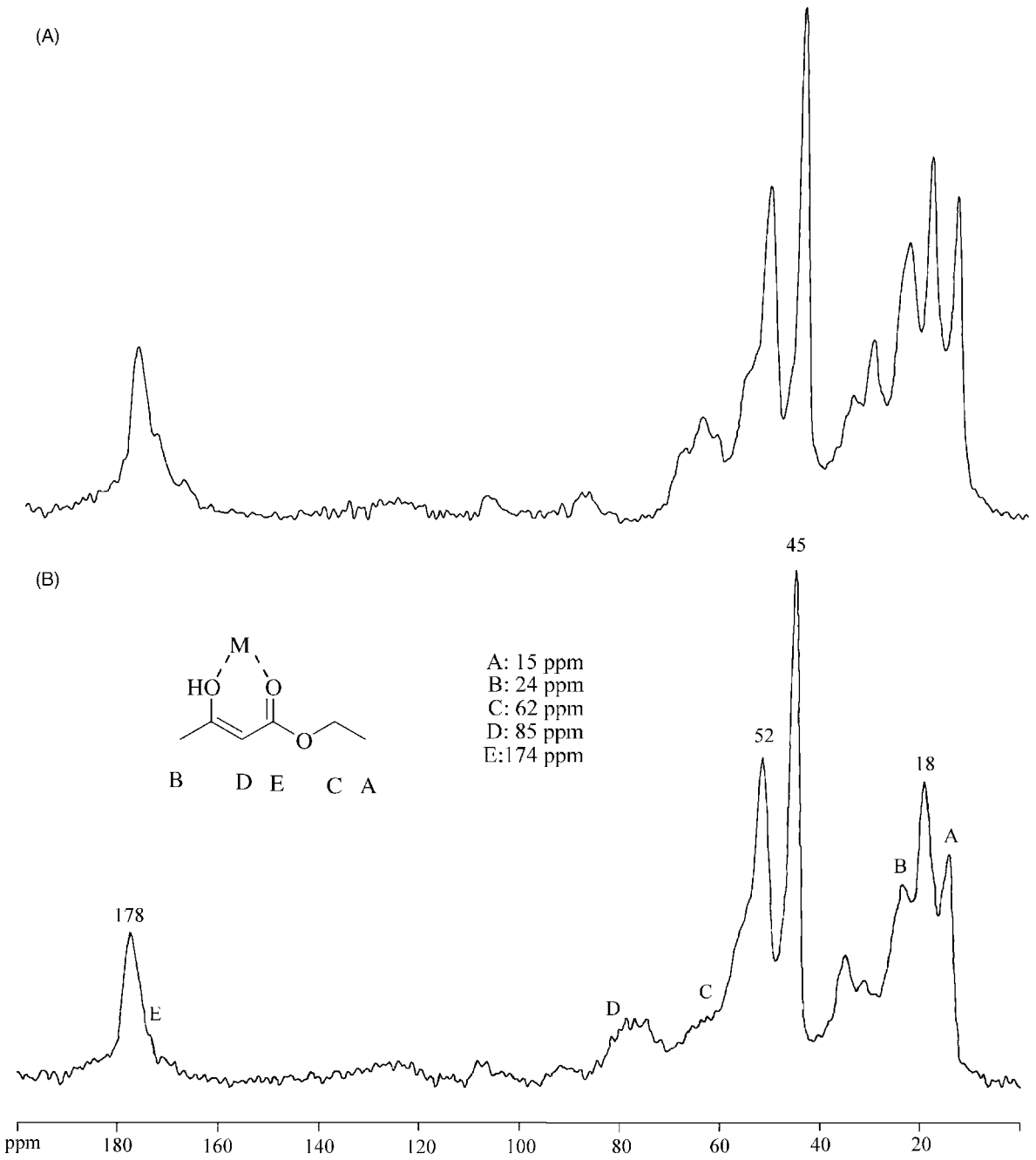

Fig. 2. ^{13}C CP/MAS NMR spectra of the hybrids: (A) M5-Zr(OBu^n)$_2$(EAA)$_2$-85; (B) M5-Ti(OBu^n)$_2$(EAA)$_2$-85.

hybrid decrease with increasing ZrO_2 content (Table 2). It implies that the motion of the EAA and PMMA segments in the M5-Zr(OBu^n)$_2$(EAA)$_2$ hybrid is more restricted to a stronger interaction with ZrO_2 and becomes tighter. The result should depend on the molecular weight (MW) of the segments [15,16] and increase with decreasing MW (chain length) [17]. Besides, it may be affected by the higher

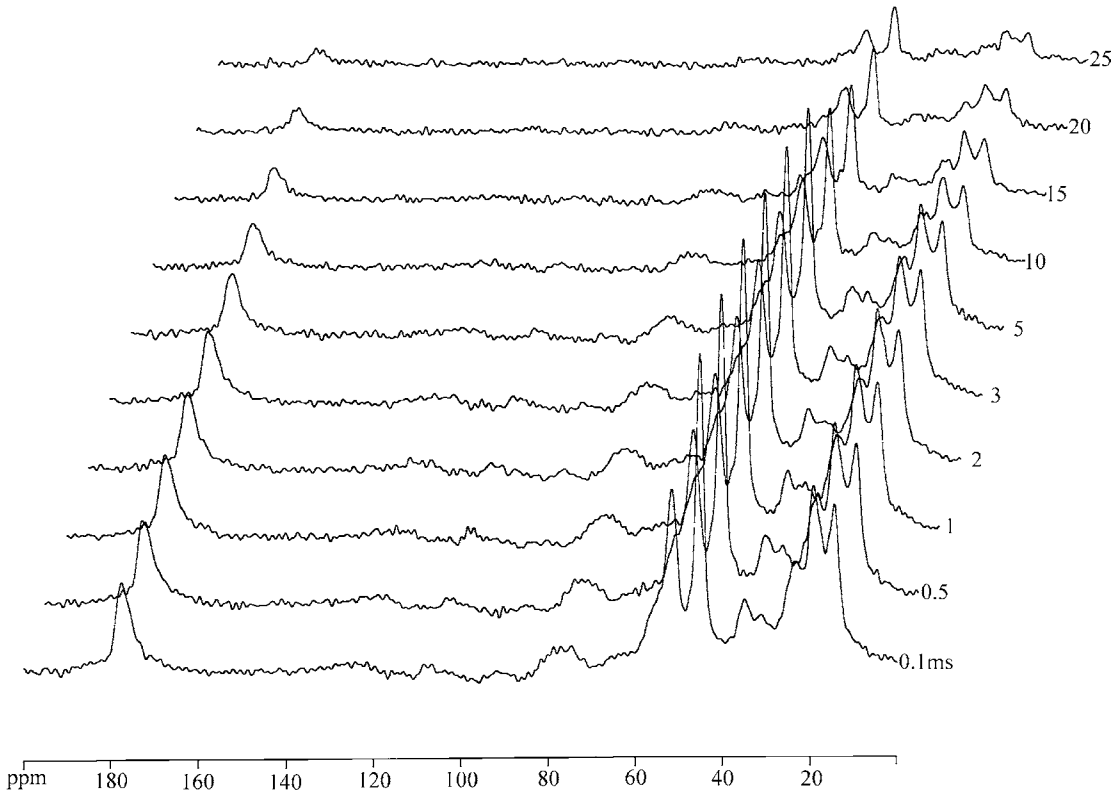

Fig. 3. Stacked plot of the ^{13}C CP/MAS NMR spectra of M5-Ti(OBu^n)$_2$(EAA)$_2$-85 hybrid as a function of delay time.

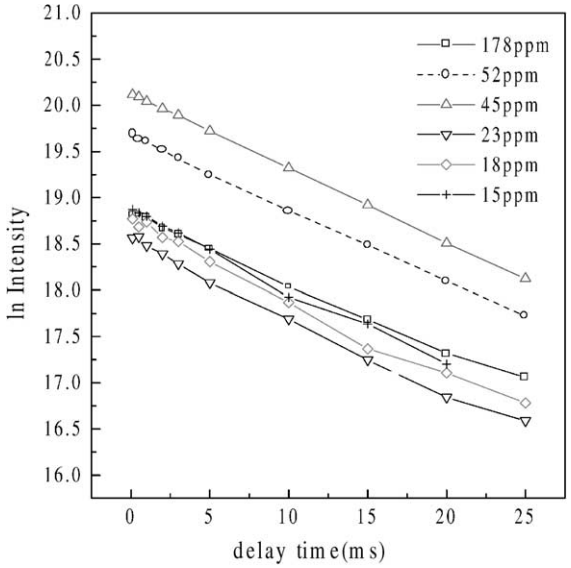

Fig. 4. Semilogarithmic plot of the peak intensity of the M5-Ti(OBu^n)$_2$(EAA)$_2$-60 hybrid as a function of delay time.

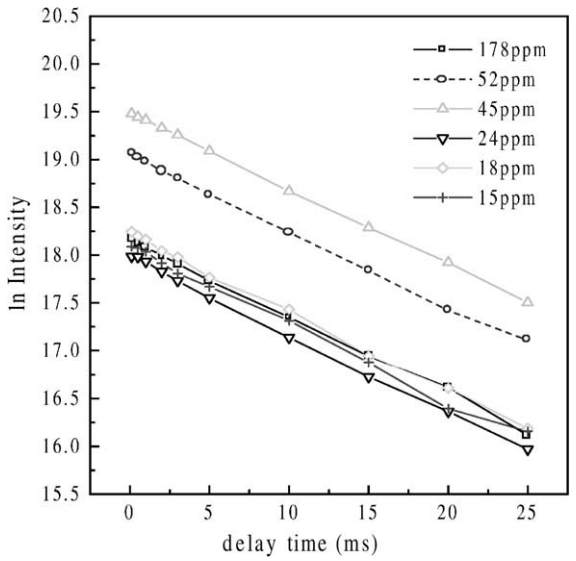

Fig. 5. Semilogarithmic plot of the peak intensity of the M5-Zr(OBu^n)$_2$(EAA)$_2$-60 hybrid as a function of delay time.

Table 2
The proton spin–lattice relaxation times in the rotating frame $T_{1\rho}^{H}$ values (ms) of the respective resonance lines (ppm) of hybrids, and the spin–diffusion path length L values (nm) of hybrids

Hybrids	$T_{1\rho}^{H}$ (EAA)			$T_{1\rho}^{H}$ (PMMA)				
	15	24	Average	18	45	52	178	Average
(A) M5-Ti(OBu^n)$_2$(EAA)$_2$-30	–	–	–	13.98	13.86	13.55	14.23	13.91 (3.8)
(B) M5-Ti(OBu^n)$_2$(EAA)$_2$-60	11.88	12.12	12.00 (3.5)	12.14	12.43	12.73	13.61	12.73 (3.6)
(C) M5-Ti(OBu^n)$_2$(EAA)$_2$-85	14.45	13.75	14.10 (3.8)	14.11	14.46	14.34	14.59	14.38 (3.8)
(D) M5-Zr(OBu^n)$_2$(EAA)$_2$-30	–	–	–	13.59	13.51	13.45	13.87	13.61 (3.7)
(E) M5-Zr(OBu^n)$_2$(EAA)$_2$-60	12.48	12.22	12.35 (3.5)	12.20	12.63	13.16	12.47	12.62 (3.6)
(F) M5-Zr(OBu^n)$_2$(EAA)$_2$-85	9.44	9.13	9.29 (3.1)	9.82	10.34	9.85	9.49	9.88 (3.1)

The values in parentheses are the spin–diffusion path length L of hybrids.

coordination number of zirconium to form a dense network structure [18].

A fast spin–diffusion occurs among all the protons in the hybrids, which averages out the whole relaxation process. Thus, the domain size of hybrids is smaller than the spin–diffusion path length within $T_{1\rho}^{H}$ time. The spin–diffusion path length can be estimated using the following equation [14]:

$$\langle L^2 \rangle = (T_{1\rho}^{H}/T_2)\langle L_0^2 \rangle \quad (2)$$

Here L_0 is the distance between protons, typically 0.1 nm, and T_2 is the spin–spin relaxation time which, below T_g, is about 10 μs, and then, the mean square distance $\langle L^2 \rangle$ over which magnetization can be evaluated. The calculated spin–diffusion path length L of EAA and PMMA segments is in the same range of 3.1–3.8 nm (Table 2). This result, therefore, implies that the PMMA segments, EAA segments and TiO_2 or ZrO_2 in hybrids are compatible in a scale of several nanometer.

3.3. Thermo-oxidative stability

The deconvoluted DTG curve of M5-Ti(OBu^n)$_2$-(EAA)$_2$-60 hybrid under air shows clearly four stages (Fig. 6). It can be seen that the peak temperatures (T_p) of each degradation is about 279, 339, 437, and 528 °C, respectively. The weight loss in the first stage (<250 °C) corresponds to the degradation of the Ti(OBu^n)$_2$(EAA)$_2$ complex, and that of in the second and third stage (250–450 °C) corresponds to PMMA [9]. On the other hand, the last step (>450 °C) may be due to the dehydroxylation of Ti–OH groups. Fig. 7 shows the TGA and DTG curves of the M5-Ti(OBu^n)$_2$-(EAA)$_2$ hybrids under air. M5-Ti(OBu^n)$_2$(EAA)$_2$ hybrids degrade mainly by a four-stage process, and that is destroyed virtually complete at 600 °C. The peak temperatures (T_{p1}) of weight loss at the first stage and the temperature (T_{max}) of maximum rate weight loss decreases with increasing the TiO_2 content (Table 3). Therefore, the former weight loss corresponds to Ti(OBu^n)$_2$(EAA)$_2$ complex and the latter corresponds to PMMA. The results imply that TiO_2 enhances the thermo-oxidation degradation of the EAA and PMMA segments. Moreover, the values of Y_c increase with increasing TiO_2 content, indicating that more three-dimensional titania network is developing as the TiO_2 proportion increases.

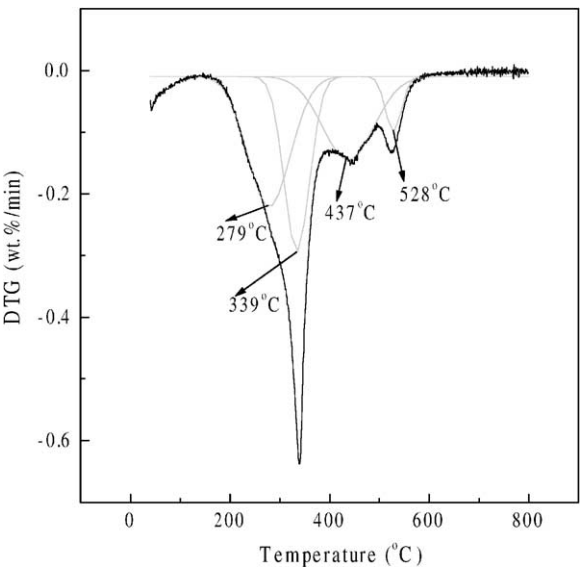

Fig. 6. The deconvoluted DTG curve of M5-Ti(OBu^n)$_2$(EAA)$_2$-60 hybrid under air.

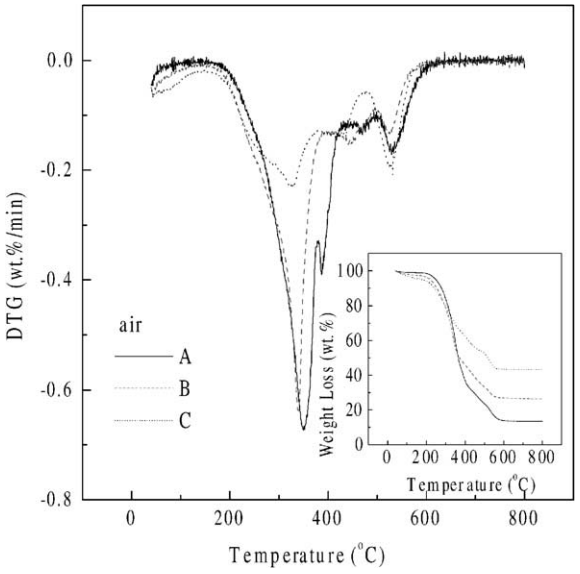

Fig. 7. TGA and DTG thermograms (10 °C/min) of hybrid materials under air: (A) M5-Ti(OBu^n)$_2$(EAA)$_2$-30; (B) M5-Ti(OBu^n)$_2$(EAA)$_2$-60; (C) M5-Ti(OBu^n)$_2$(EAA)$_2$-85.

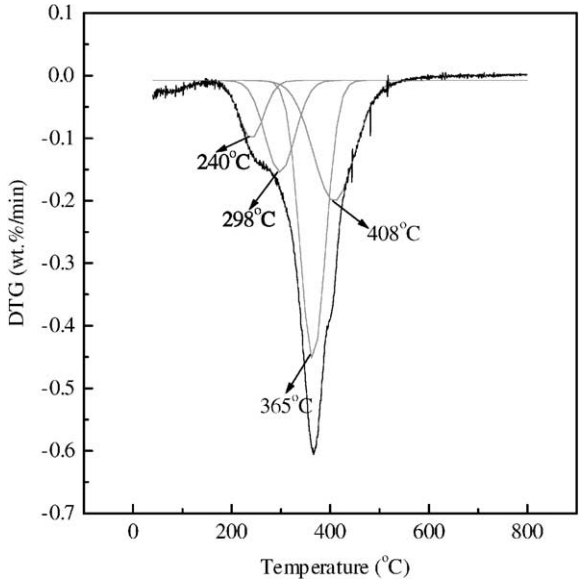

Fig. 8. The deconvoluted DTG curve of M5-Zr(OBu^n)$_2$(EAA)$_2$-60 hybrid under air.

The thermo-oxidative degradation of the M5-Zr(OBu^n)$_2$(EAA)$_2$-60 hybrid (Fig. 8) from the first to third step is similar to that of the M5-Ti(OBu^n)$_2$(EAA)$_2$-60 hybrid, and the last step may be due to the dehydroxylation of ZrOH groups [19]. Fig. 9 shows the TGA and DTG curves of the M5-Zr(OBu^n)$_2$(EAA)$_2$ hybrids under air at a heating rate of 10 °C/min. Table 3 lists the T_{p1} and T_{max} values of the thermo-oxidative degradation of the M5-Zr(OBu^n)$_2$(EAA)$_2$ hybrids. The T_{p1} value of the M5-Zr(OBu^n)$_2$(EAA)$_2$ hybrids decreases with increasing ZrO_2 content, while the value of T_{max} is around 367 °C. The results imply that the ZrO_2 enhances the degradation of the EAA ligand.

Fig. 10 shows the TGA and DTG curves of the M5-Al(OBu^s)$_2$(EAA)$_2$-60, M5-Ti(OBu^n)$_2$(EAA)$_2$-60 and M5-Zr(OBu^n)$_2$(EAA)$_2$-60 hybrids under air. The T_{max} value of the hybrids is in the order M5-Al(OBu^s)(EAA)$_2$-60 < M5-Ti(OBu^n)$_2$(EAA)$_2$-60 < M5-Zr(OBu^n)$_2$(EAA)$_2$-60 hybrid. The results reveal that the latter has the more stable structure between metal oxide and PMMA segment. Thus, the apparent activation energy (E_a) for the hybrids in thermo-oxidative degradation of the PMMA segment may be in the order M5-Al(OBu^s)(EAA)$_2$ < M5-Ti(OBu^n)$_2$-(EAA)$_2$ < M5-Zr(OBu^n)$_2$(EAA)$_2$. Moreover, the M5-Zr(OBu^n)$_2$(EAA)$_2$-60 hybrid has the higher Y_c value,

Table 3
The characteristic parameters of thermo-oxidative degradation (10 °C/min) for hybrid materials

Hybrids	T_{p1} (°C)	T_{max} (°C)	E_a (kJ/mol)[a]	Y_c (wt.%)
(A) M5-Ti(OBu^n)$_2$(EAA)$_2$-30	279	349	68	13.6
(B) M5-Ti(OBu^n)$_2$(EAA)$_2$-60	279	339	60	26.4
(C) M5-Ti(OBu^n)$_2$(EAA)$_2$-85	268	329	31	43.3
(D) M5-Zr(OBu^n)$_2$(EAA)$_2$-30	283	365	75 (58)[a]	14.2
(E) M5-Zr(OBu^n)$_2$(EAA)$_2$-60	280	366	74 (43)	28.3
(F) M5-Zr(OBu^n)$_2$(EAA)$_2$-85	259	369	61 (34)	44.4

T_{p1} is the temperature of maximum rate of weight loss at the first stage in fitting curve; T_{max} the maximum rate temperatures of weight loss; E_a the activation energy of degradation; Y_c the char yield at 800 °C.

[a] The values in parentheses are the E_a values of thermo-oxidative degradation of M5-Al(OBu^s)(EAA)$_2$ hybrids.

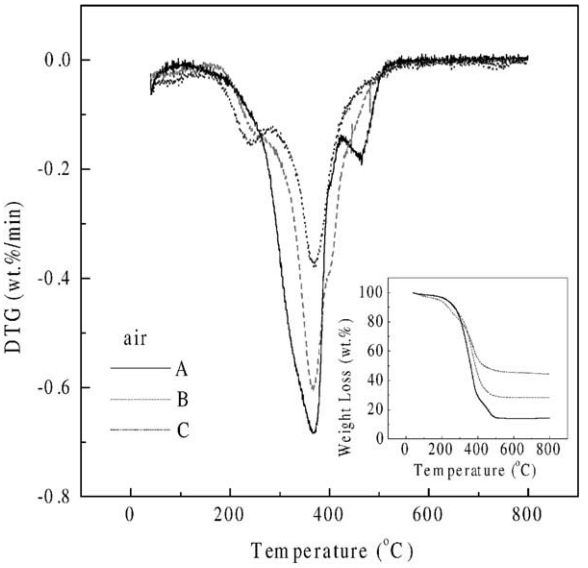

Fig. 9. TGA and DTG thermograms (10 °C/min) of hybrid materials under air: (A) M5-Zr(OBu^n)$_2$(EAA)$_2$-30; (B) M5-Zr(OBu^n)$_2$(EAA)$_2$-60; (C) M5-Zr(OBu^n)$_2$(EAA)$_2$-85.

indicating that ZrO_2 retards carbonization of PMMA and increases pyrolysis residue.

The reaction order (n) of the thermo-oxidative degradation in the first stage, determined by the Kissinger's equation [20], is independent of the PMMA content and that is about 1.26. Fig. 11 shows the logarithmic plot for degradation rate $g(\alpha)$ of the hybrids versus temperature in the stage of random scission for the PMMA segments. Table 3 lists the apparent activation energy E_a of the degradation, evaluated from van Krevelen's method [9]. The E_a values of random scission for the PMMA segments decrease with increasing metal oxide, and the E_a value of hybrids is in the order M5-Ti(OBu^n)$_2$(EAA)$_2$ < M5-Zr(OBu^n)$_2$(EAA)$_2$. It is reasonable to correlate that with the degree of restriction of mobility as mentioned. Moreover, the reduction in E_a in the M5-Ti(OBu^n)$_2$(EAA)$_2$ hybrids is larger than that in the M5-Zr(OBu^n)$_2$(EAA)$_2$ hybrids. At present, the reduction may be rationalized on the basis of the thermal conductivity of the metal oxide in the order ZrO_2 (2 W/(m K) at 100 °C) < TiO_2 (6.5 W/(m K) at 100 °C) [21].

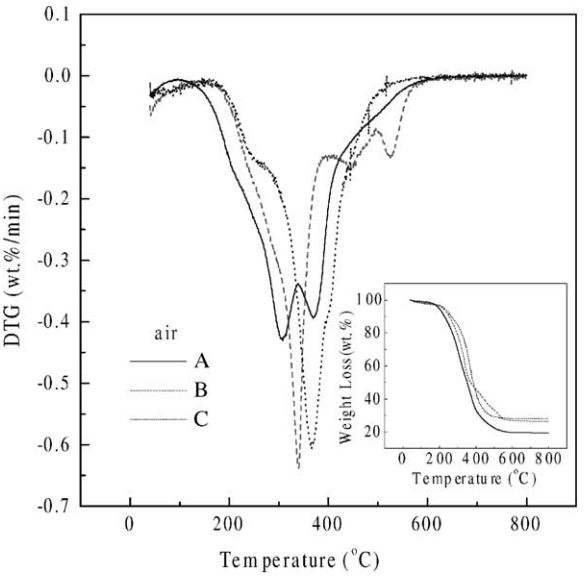

Fig. 10. TGA and DTG thermograms (10 °C/min) of hybrid materials under air: (A) M5-Al(OBu^s)(EAA)$_2$-60; (B) M5-Ti(OBu^n)$_2$(EAA)$_2$-60; (C) M5-Zr(OBu^n)$_2$(EAA)$_2$-60.

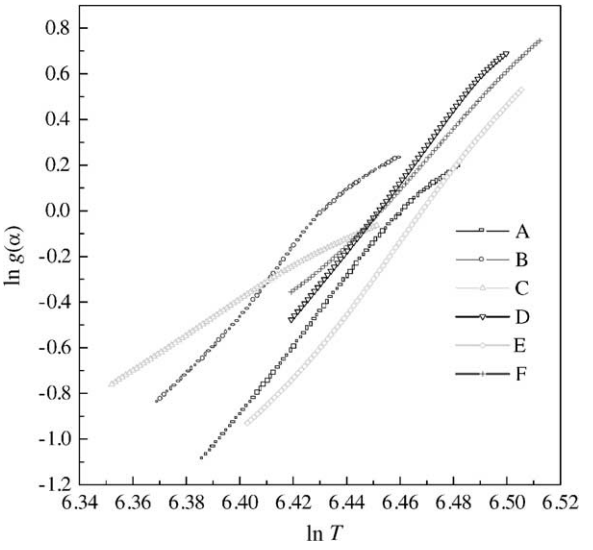

Fig. 11. Plot of ln $g(\alpha)$ vs. ln T for thermo-oxidative degradation (10 °C/min) of the hybrids: (A) M5-Ti(OBu^n)$_2$(EAA)$_2$-30; (B) M5-Ti(OBu^n)$_2$(EAA)$_2$-60; (C) M5-Ti(OBu^n)$_2$(EAA)$_2$-85; (D) M5-Zr(OBu^n)$_2$(EAA)$_2$-30; (E) M5-Zr(OBu^n)$_2$(EAA)$_2$-60; (F) M5-Zr(OBu^n)$_2$(EAA)$_2$-85.

4. Conclusions

The M5-Ti(OBu^n)(EAA)$_2$ and M5-Zr(OBu^n)-(EAA)$_2$ hybrids were prepared via sol–gel techniques by mixing PMMA, titanium and zirconium n-butoxide modified with ethyl acetoacetate. The characterization

of the hybrids was confirmed through IR, ^{13}C, NMR and TGA. The $T_{1\rho}^{H}$ values of the M5-Ti$(OBu^n)_2(EAA)_2$ hybrid were not affected by metal oxide content, while that of M5-Zr$(OBu^n)_2(EAA)_2$ hybrid decreased with increasing ZrO_2 content. The observation implied that the motion of the EAA and PMMA segments in the M5-Zr$(OBu^n)_2(EAA)_2$ hybrid was more restricted to a stronger interaction with ZrO_2 and becomes tighter. The result might be affected by the higher coordination number of zirconium to form a dense network structure. The thermo-oxidative stability of the PMMA moiety in hybrids was affected by the kind of metal alkoxide. The apparent activation energy E_a for random scission of PMMA segments in hybrids decreased with increasing the metal oxide content. The reduction in E_a in the M5-Ti$(OBu^n)_2(EAA)_2$ hybrids was larger than that of in the M5-Zr$(OBu^n)_2$-$(EAA)_2$ hybrids, and it may be rationalized on the basis of the thermal conductivity of the metal oxide in the order $ZrO_2 < TiO_2$.

Acknowledgements

The authors thank the National Science Council of the Republic of China (Grant NSC 90-2113-M014-001). We would also like to thank Miss S.Y. Fang and Mr. Y.C. Lin for their expert technical assistance.

References

[1] M. Atik, J. Zarzycki, C. R'kha, J. Mater. Sci. Lett. 13 (1994) 266.
[2] K. Terabe, K. Kato, H. Miyazaki, S. Yamaguchi, A. Imai, Y. Iguchi, J. Mater. Sci. 29 (1994) 1617.
[3] W. Que, W.G. Liu, Y. Zhou, Y.L. Lam, Y.C. Chan, S.D. Cheng, H.P. Li, Y.W. Chen, S. Buddhudu, C.H. Kam, Mater. Lett. 44 (2000) 309.
[4] W. Que, Y. Zhou, Y.L. Lam, Y.C. Chan, C.H. Kam, Thin Solid Films 358 (2000) 16.
[5] W. Que, Z. Sun, Y. Zhou, Y.L. Lam, Y.C. Chan, C.H. Kam, Thin Solid Films 359 (2000) 177.
[6] J. Zhang, S.C. Luo, L.L. Gui, J. Mater. Sci. 32 (1997) 1469.
[7] W.C. Chen, S.J. Lee, L.H. Lee, J.L. Lin, J. Mater. Chem. 9 (1999) 2999.
[8] T.C. Chang, Y.T. Wang, Y.S. Hong, Y.S. Chiu, Thermochim. Acta 372 (2001) 165.
[9] D.W. van Krevelen, C. van Heerden, F. Huntjens, J. Fuel 30 (1951) 253.
[10] S. Katyama, I. Yoshinaga, N. Yamada, Sol–gel optics IV, Proc. SPIE 3136 (1997) 134.
[11] J. Livage, C. Sanchez, J. Non-Cryst. Solids 145 (1992) 11.
[12] T.C. Chang, Y.T. Wang, Y.S. Hong, Y.S. Chiu, J. Polym. Sci.: Part A: Polym. Chem. 38 (2000) 1972.
[13] T.C. Chang, Y.T. Wang, Y.S. Hong, C.T. Liu, Phosphorus, Sulfur and Silicon 167 (2000) 47.
[14] M. Mehring, Principles of High Resolution NMR in Solids, 2nd Edition, Springer, Berlin, 1983, p. 260.
[15] S. Bistac, P. Kunemann, J. Schultz, Polymer 39 (1998) 4875.
[16] P.D. Hong, J.H. Chen, Polymer 39 (1998) 5809.
[17] V.A. Bershtein, L.M. Egorova, P.N. Yakushev, G. Georgoussis, A. Kyritsis, P. Pissis, P. Sysel, L. Brozova, Macromol. Symp. 146 (1999) 9.
[18] N. Yamada, I. Yoshinaga, S. Katyama, J. Mater. Res. 14 (1999) 1720.
[19] F. Rubio, J. Rubio, J.L. Oteo, Thermochim. Acta 320 (1998) 231.
[20] H.H.E. Kissinger, Anal. Chem. 29 (1957) 1702.
[21] D.R. LiDe (Ed.), Handbook of Chemistry and Physics, 75th Edition, CRC Press, Florida, 1994, p. 12–19.